Crucial Role of the Lattice Distortion in the Magnetism of $LaMnO_3$

Igor Solovyev,[1,*] Noriaki Hamada,[1] and Kiyoyuki Terakura[2]
[1]*Joint Research Center for Atom Technology, Angstrom Technology Partnership, 1-1-4 Higashi, Tsukuba, Ibaraki 305, Japan*
[2]*Joint Research Center for Atom Technology, National Institute for Advanced Interdisciplinary Research, 1-1-4 Higashi,Tsukuba, Ibaraki 305, Japan*
(Received 27 November 1995)

The stability of the *A*-type antiferromagnetic order and canted magnetic structure of $LaMnO_3$ perovskite is explained in the itinerant-electron picture based on the local-spin-density approximation. We demonstrate the crucial role of the observed lattice distortion which strongly affects the magnetocrystalline anisotropy, as well as the anisotropic and isotropic exchange interactions in this compound. [S0031-9007(96)00499-1]

PACS numbers: 75.25.+z, 71.70.Ej, 71.70.Gm, 75.40.Mg

A huge negative magnetoresistance observed near room temperature [1] and the structural phase transition induced by an external magnetic field [2] in the perovskite Mn oxides $La_{1-x}D_xMnO_3$ with D= Ca, Sr, Ba have been subjects of very intensive experimental and theoretical studies for the last few years. Traditionally, all the physics controlling the basic properties of the systems was believed to be included in the "double-exchange" model [3]. Nevertheless, it was shown recently [4] that the latter is incompatible with many aspects of experimental data. The importance of other ingredients such as the electron-phonon interaction causing the Jahn-Teller splitting of e_g levels [4] and the on-site Coulomb correlations together with antiferromagnetic (AFM) exchange interactions involving t_{2g} states [5] has been suggested.

In the present work, we present a detailed analysis of lattice effects on the magnetic behavior of the parent compound $LaMnO_3$ by using the local-spin-density approximation (LSDA). The perovskite transition-metal oxides are generally considered as highly correlated systems. However, it was demonstrated recently [6,7] that many aspects of the ground state as well as single-electron excited-state properties of $LaMnO_3$ can be fairly well described in the LSDA band calculations. Moreover, using the LDA $+U$ approach we showed in [7] that the localized picture for magnetic behavior, where the appearance of local moments is driven by the large on-site Coulomb interaction, is in serious contradiction to the occurrence of an AFM ground state for $LaMnO_3$. Here we will explicitly show that the Jahn-Teller distortion (JTD) plays a crucial role in the stability of the *A*-type AFM ground state [8]. Furthermore, we will demonstrate that finer details of the magnetic behavior, such as magnetic easy axis and small canting of magnetic moments, both originating from the interplay between the spin-orbit interaction (SOI) and the lattice distortion, can be successfully treated by the LSDA band calculations.

Since the pioneering works of Dzyaloshinsky and Moriya [9], the SOI has been well known to be one of the sources responsible for noncollinear magnetism, and yet the attempts of first principles calculations for this effect were made only recently [10]. We show how this problem can be treated using the perturbation theory and Green's function technique in the real space.

Let us assume that without SOI the ground state corresponds to the collinear arrangement of the (spin) magnetic moments. Any rigid rotation of the spins for the whole system can be described by a unitary transformation of Green's function in the spin subspace: $\tilde{G}_0(\vartheta,\varphi) = U_S^{\dagger}(\vartheta,\varphi)G_0U_S(\vartheta,\varphi)$, where the angles (ϑ,φ) define the orientation of the spin magnetization in the global system $\tilde{\mathbf{e}}_0 = (\sin\vartheta\cos\varphi, \sin\vartheta\sin\varphi, \cos\vartheta)$. The energy is invariant with respect to such operations. Then, we introduce two kinds of perturbations. (i) Small deviation of the spin magnetization near $\tilde{\mathbf{e}}_0$ at the site i: $\tilde{\mathbf{e}}^i = \tilde{\mathbf{e}}_0 + \Delta\tilde{\mathbf{e}}^i$. The corresponding change of the one-electron potential can be expressed as $\Delta V^i_{\rm ex} = B^i\Delta\tilde{\mathbf{e}}^i\boldsymbol{\sigma}$, where B^i is the exchange field expressed in terms of LSDA spin-up and spin-down potentials at the site i as $B = 1/2(V^{\uparrow} - V^{\downarrow})$ and $\boldsymbol{\sigma}$ is the vector of Pauli matrices. (ii) The spin-orbit interaction $\Delta V^i_{\rm so} = 1/2\sum_l \xi^i_\ell \mathbf{L}\boldsymbol{\sigma}$. In the lowest orders of perturbation theory, by using the local-force theorem, the total energy change δE near the equilibrium corresponding to the scalar-relativistic approach, can be transformed to

$$\delta E = E_H + E_{\rm DM} + E_{\rm MAE}. \tag{1}$$

The first term $E_H \simeq -1/2\sum_{ij} J_{ij}\tilde{\mathbf{e}}^i\tilde{\mathbf{e}}^j$ describes isotropic Heisenberg exchange interactions between spin magnetic moments and appears in the second order of perturbation with respect to $\Delta V_{\rm ex}$ [11]. The magnetocrystalline anisotropy energy (MAE) first appears in the second-order expansion with respect to $\Delta V_{\rm so}$ and can also be expressed in terms of intra-atomic and interatomic interaction energies $E_{\rm MAE} = \sum_{ij}\varepsilon_{ij}(\vartheta,\varphi)$ [12]. The antisymmetric anisotropic Dzyaloshinsky-Moriya (DM) coupling $E_{\rm DM} \simeq \sum_{i>j}\mathbf{d}_{ij}[\tilde{\mathbf{e}}^i \times \tilde{\mathbf{e}}^j]$, corresponding to the mixed type perturbation of the order $\Delta V_{\rm ex}\Delta V_{\rm so}$, can be

expressed through $\mathbf{f}_i^j = [\mathbf{d}_{ij} \times \tilde{\mathbf{e}}_0]$, where

$$\mathbf{f}_i^j = -\frac{1}{\pi}\,\mathrm{Im}\int_{-\infty}^{E_F} dE \times \mathrm{Tr}_L\Big[\boldsymbol{\sigma}(B^j \tilde{G}_0^{ji}\Delta V_{\mathrm{so}}^i \tilde{G}_0^{ij} - B^i \tilde{G}_0^{ij}\Delta V_{\mathrm{so}}^j \tilde{G}_0^{ji})\Big], \quad (2)$$

and Tr_L runs over the orbital variables. Note that $\mathbf{f}_i^j \simeq \mathbf{d}_{ij} \times \tilde{\mathbf{e}}^j$ is the magnetic force acting on the magnetic moment at the site i created by that at the site j.

The crystal structure of $LaMnO_3$ shows two principal types of distortions: the local tetragonal JTD of oxygen atoms around each Mn site [13], which is periodically arranged as shown in Fig. 1, and tilting of MnO_6 octahedra resulting in the orthorhombic D_{2h}^{16} superstructure [14] with four formula units in the primitive cell. The strength of the crystal distortion appears to be sufficient to split e_g states around E_F, creating the band gap and the orbital ordering in the LSDA calculations (Fig. 1).

We have calculated the parameters J_{ij}, $\mathbf{d}_{ij}$, and ε_{ij} associated with $3d$ states of Mn atoms in the AFM A-type configuration by using the ASA-LMTO method [15,16].

First, we want to show that the JTD is responsible for the A-type AFM ordering of the $LaMnO_3$. As shown in Table I, the first neighbor in-plane exchange $J_{\mathbf{ab}}^1$ decreases with the lattice distortions. However, $J_{\mathbf{ab}}^1$ still has a considerable magnitude with the positive sign, being consistent with the A-type AFM order. The effects of the lattice distortion on the first neighbor interplane exchange coupling $J_{\mathbf{c}}^1$ is more dramatic. In order to understand the role of pure JTD we have performed a series of calculations, changing only the strength of the local tetragonal distortion and neglecting the tilting deformation. If the total volume of crystal remains unchanged, the structural modification can be described by only one parameter $R_t = d_L/d_S$, where d_L and d_S are the long and the short Mn-O bond lengths in the distorted MnO_6 octahedron. The experimental structure clearly shows the long Mn-O bond with $d_L = 2.19$ Å and two slightly different short bonds with $d_S = 1.90$ and 1.96 Å. Thus, the magnitude of experimental JTD can be evaluated as $R_t \sim 1.13$. Figure 2 shows $J_{\mathbf{c}}^1$ versus R_t obtained for the experimental volume of $LaMnO_3$. Without tilting, there is no mixing between t_{2g} and e_g states in the nearest neighbor transfer integrals in the perovskite lattice. Thus, t_{2g} and e_g contributions in $J_{\mathbf{c}}^1$ can be considered separately. As expected for the half-filled t_{2g} band [17], the t_{2g}-type interatomic exchange reveals AFM behavior, and its absolute value monotonously increases as the distance between nearest Mn atoms along the **c** direction decreases with the JTD. On the contrary, JTD significantly reduces the e_g type interplane exchange. Generally, the e_g exchange (both in-plane and interplane) slightly decreases with increasing the splitting between occupied and empty states. More importantly, the *type* of occupied and empty states related with the orbital ordering strongly influences the e_g exchange interactions. In order to illustrate it, we further decompose the e_g exchange in terms of partial contributions from $3x^2 - r^2$ and $y^2 - z^2$ type orbitals split by JTD (Fig. 1). Without JTD, using simple tight-binding arguments [17], it is easy to see that for the quarter-filled e_g band all interactions related with these orbitals are positive. Along the **c** axis only the weak $(3x^2 - r^2) - (3x^2 - r^2)$ interaction [18] becomes AFM with JTD, whereas both $(3x^2 - r^2) - (y^2 - z^2)$ and the strongest $(y^2 - z^2) - (y^2 - z^2)$ interactions remain positive. The last term is the most sensitive to the strength of JTD and mainly determines the behavior of the e_g interplane exchange. Increase of the JTD leads to emptying of $(y^2 - z^2)$ orbitals and systematically decreases the contribution of this type in the $J_{\mathbf{c}}^1$ (Fig. 2). Nevertheless, even

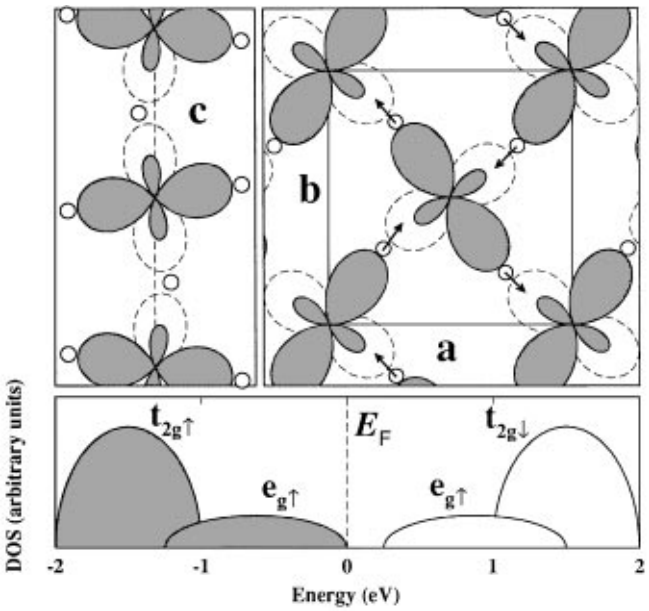

FIG. 1. Upper panel: Orbital ordering along the **c** axis and in the **a**-**b** plane of the orthorhombic cell. Shaded orbits denote occupied e_g states of $3x^2 - r^2$ and $3y^2 - r^2$ symmetry, and orbits with broken lines denote empty e_g states of $y^2 - z^2$ and $x^2 - z^2$ symmetry. Local displacements of oxygen atoms are shown by arrows. Lower panel: schematical position of $t_{2g\uparrow,\downarrow}$ bands and $e_{g\uparrow}$ band split by JTD in the LSDA band calculations (Ref. [6]).

TABLE I. Isotropic exchange interaction parameters (J_{ij}) as obtained for cubic and experimental orthorhombic structure of $LaMnO_3$ (in mRy). The subscripts **ab** and **c** denote "in-plane" and "interplane," and subscripts 1 and 2 the first and second neighborhood. Atomic positions 1, 2, 3, and 4 are shown in Fig. 3.

ij	Type	Cubic	Orthorhombic
13	$J_{\mathbf{ab}}^1$	2.13	0.67
12	$J_{\mathbf{c}}^1$	2.13	0.23
23	$J_{\mathbf{c}}^2$	−0.18	−0.25
14	$J_{\mathbf{c}}^2$	−0.18	−0.21

for sufficiently large distortions, the total e_g exchange remains positive. Thus, in order to explain the magnetic behavior of $LaMnO_3$, both t_{2g} and e_g interatomic exchanges are important. Without JTD, the positive e_g-type exchange prevails over the negative t_{2g} one and the system remains ferromagnetic. $J^1_{\mathbf{c}}$ changes its sign around $R_t \sim 1.12$, which is close to experimental JTD. For the experimental structure, $J^1_{\mathbf{c}}$ is weakly ferromagnetic and comparable with the AFM second neighbor interplane exchanges $J^2_{\mathbf{c}}$ (Table I). Taking into account the coordination numbers, we have $2J^1_{\mathbf{c}} + 8J^2_{\mathbf{c}} \simeq -1.4$ mRy, and the A-type antiferromagnetism of $LaMnO_3$ associated with the JTD is thereby explained.

Let us discuss next the behavior of MAE. As applied to $LaMnO_3$ we would like to emphasize two aspects of this problem. (i) For undistorted cubic perovskites the MAE is generally small because the leading second-order contribution with respect to the SOI will vanish by the symmetry rules. The crystal distortion, which is very large in $LaMnO_3$, shall clearly enhance the MAE effect. (ii) Orthorhombic AFM $LaMnO_3$ is an *insulator* (Fig. 1) where the direct gap ~ 0.7 eV is at least one order of magnitude larger than the strength of SOI. Therefore, the quasidegeneracy of states close to E_F plays only a minor role, and the real space expansion of the MAE [12] is well justified. Moreover, we found that the site-diagonal components of the MAE expansion $\varepsilon_{ii}(\vartheta, \varphi)$, are almost 2 orders of magnitude larger than nondiagonal ones. The angular behavior of the $\varepsilon_{ii}(\vartheta, \varphi)$ term in the **a**-**b** plane is very much reminiscent of the distribution of the occupied $(3x^2 - r^2)/(3y^2 - r^2)$ type orbitals (Fig. 1); around each Mn site the minimum of the single-ion MAE is directed along the longest Mn-O bond. It can be easily understood in the simple ionic picture, where the angular part of the MAE due to the interaction between occupied $e_{g\uparrow}$ states, say, $3x^2 - r^2$ symmetry stabilized by the local distortions, and empty $t_{2g\downarrow}$ states (Fig. 1) is proportional to $3\sin^2\vartheta\cos^2\varphi - 1$. The same is true for the couple of occupied $t_{2g\uparrow}$ and empty $e_{g\uparrow}$ states of $y^2 - z^2$ symmetry. Thus, the single-ion MAE terms strictly follow the orbital ordering associated with the JTD. The magnitude of the single-ion MAE, being directly related with the strength of JTD, is very large for the experimental structure: 0.069 mRy, being comparable with perpendicular MAE of some layered compounds. Finally, rotation of the MnO_6 octahedra in the **a**-**b** plane, which has opposite direction for different Mn sites (Fig. 1), slightly tilts the single-ion MAE minima toward the **b** axis, making it the global easy magnetization direction in $LaMnO_3$.

The structure of the anisotropic superexchange interaction between nearest Mn sites is shown in Fig. 3. The components of $\mathbf{d}_{ij}$ along the **a**, **b**, and **c** axes are given in the parentheses attached to the oxygen atom connecting the two neighboring Mn atoms. The behavior of the anisotropic exchange obeys the general symmetry rules. The orthorhombic space group D^{16}_{2h} contains three 180° rotations around **a**, **b**, and **c** associated with translations of $(\mathbf{a}/2, \mathbf{b}/2, 0)$, $(\mathbf{a}/2, \mathbf{b}/2, \mathbf{c}/2)$, and $(0, 0, \mathbf{c}/2)$, respectively. In combination with antisymmetry of the DM exchange $\mathbf{d}_{ij} = -\mathbf{d}_{ji}$, it gives (i) $\gamma_{\mathbf{c}} = 0$ for the first neighbor interplane exchange; (ii) the interaction with four nearest Mn neighbors in the **a**-**b** plane is characterized by the same $\beta_{\mathbf{ab}}$ and $\gamma_{\mathbf{ab}}$ components, whereas $\alpha_{\mathbf{ab}}$ alters

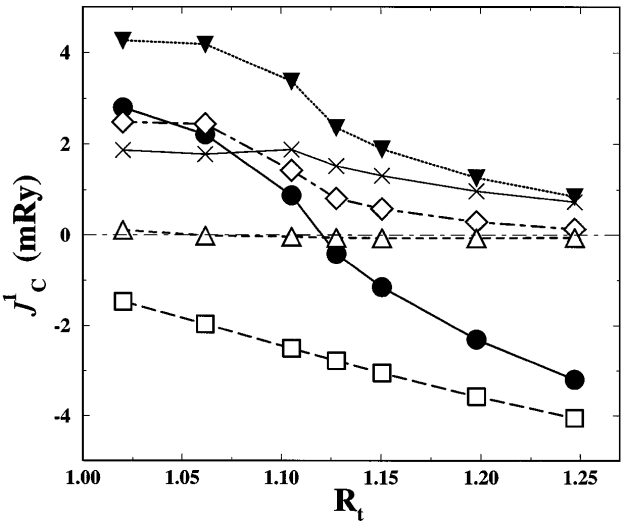

FIG. 2. First neighbor isotropic interplane exchange as a function of local tetragonal distortion: total $3d$ (filled circles), total t_{2g} (squares), total e_g (filled triangles), $(y^2 - z^2) - (y^2 - z^2)$ (diamonds), $(3x^2 - r^2) - (y^2 - z^2)$ (crosses), and $(3x^2 - r^2) - (3x^2 - r^2)$ (open triangles).

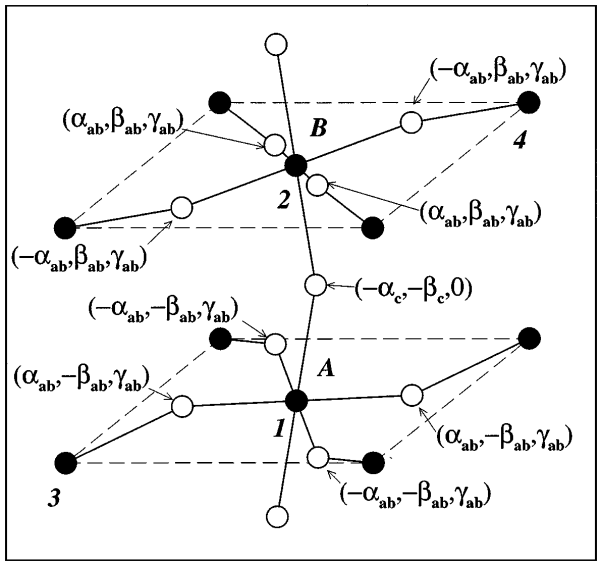

FIG. 3. Anisotropic exchange parameters associated with different Mn-O-Mn bonds (black and white spheres are Mn and O, respectively). α, β, and γ are the components of $\mathbf{d}_{ij}$ vectors along **a**, **b**, and **c**. For the interplane exchange $\alpha_{\mathbf{c}}$=0.032 mRy and $\beta_{\mathbf{c}}$=0.052 mRy. For the in-plane exchange $\alpha_{\mathbf{ab}}$=0.032 mRy, $\beta_{\mathbf{ab}}$=0.024 mRy, and $\gamma_{\mathbf{ab}}$=0.039 mRy.

the sign. For second neighbors in the **a**-**b** plane, separated by primitive translations, $\mathbf{d}^2_{\mathbf{ab}} = 0$. The second neighbor interplane DM exchanges were found to be at least one order of magnitude smaller than those for the first neighbors and can be neglected.

Having estimated parameters of magnetic interactions, the equilibrium magnetic structure for $LaMnO_3$ can be found. First, the isotropic exchange, being the strongest magnetic interaction, forms the main framework—AFM *A*-type ordering. Second, the spin magnetic moments are confined along the **b** axis by the magnetocrystalline anisotropy. Thus, for two planes *A* and *B* shown in Fig. 3, we can assume $\tilde{\mathbf{e}}^A_0 = (0, 1, 0)$ and $\tilde{\mathbf{e}}^B_0 = (0, -1, 0)$. Third, the DM exchange produces small noncollinearity of spin magnetic moments. Considering the interplane anisotropic exchange between sites 1 and 2 (Fig. 3), the force is given by $\mathbf{f}^2_1 = \mathbf{d}_{12} \times \tilde{\mathbf{e}}^B_0 = (0, 0, \alpha_{\mathbf{c}})$. Since $\mathbf{d}_{21} = -\mathbf{d}_{12}$ and $\tilde{\mathbf{e}}^A_0 = -\tilde{\mathbf{e}}^B_0$, we have $\mathbf{f}^1_2 = \mathbf{f}^2_1$. The forces due to interaction with four nearest neighbors in the same plane are $\mathbf{f}^B_2 = 4(\gamma_{\mathbf{ab}}, 0, 0)$, $\mathbf{f}^A_3 = \mathbf{f}^B_2$, and $\mathbf{f}^A_1 = \mathbf{f}^B_4 = -\mathbf{f}^B_2$. Therefore, the interplane DM exchange gives rise to the **c** component of spin magnetic moment being the same for all Mn sites, and responsible for the weak ferromagnetism in $LaMnO_3$. The in-plane interaction results in nonvanishing components of the spin magnetic moments along the **a** axis, whose mutual orientation obeys the *G*-type AFM ordering [8]. This magnetic structure is consistent with results of the phenomenological magnetic space group considerations [19]. In order to obtain the quantitative picture, we minimize the energy given by Eq. (1) with respect to the orientations of Mn($3d$) magnetic moments $\{\mathbf{e}^i\}$. It leads to the magnetic structure described above, where the **a**, **b**, and **c** components of the spin (orbital) magnetic moments at the same site, say 1 in Fig. 3, are in μ_B –0.090 (0.010), 3.620 (–0.011), and 0.105 (–0.003), respectively. In addition to the large AFM **b** component $(3.7 \pm 0.1)\mu_B$, a weak ferromagnetic **c** component $\sim 0.1\mu_B$ has been reported experimentally [14]. Both are in good agreement with our calculations. Finally, due to the low symmetry, the spin and orbital magnetic moments at the same site are not collinear.

In summary, we have calculated magnetic interaction parameters for $LaMnO_3$ by using the LSDA approach and found them to be strongly affected by the lattice distortions.

The present work was partly supported by New Energy and Industrial Technology Development Organization (NEDO) and also by the Grant-in-Aid for Scientific Research from the Ministry of Education, Science and Culture of Japan.

*On leave from Institute of Metal Physics, Ekaterinburg,Russia. Electronic address: igor@jrcat.or.jp

[1] R. von Helmolt *et al.*, Phys. Rev. Lett. **71**, 2331 (1993); A. Urushibara *et al.*, Phys. Rev. B **51**, 14 103 (1995).

[2] A. Asamitsu *et al.*, Nature (London) **373**, 407 (1995).

[3] C. Zener, Phys. Rev. **82**, 403 (1951); P. W. Anderson and H. Hasegawa, Phys. Rev. **100**, 675 (1955); P.-G. de Gennes, Phys. Rev. **118**, 141 (1960).

[4] A. J. Millis, P. B. Littlewood, and B. I. Shraiman, Phys. Rev. Lett. **74**, 5144 (1995).

[5] J. Inoue and S. Maekawa, Phys. Rev. Lett. **74**, 3407 (1995).

[6] N. Hamada, H. Sawada, and K. Terakura, in *Spectroscopy of Mott Insulators and Correlation Metals*, edited by A. Fujimori and Y. Tokura (Springer-Verlag, Berlin, 1995); D. D. Sarma *et al.*, Phys. Rev. Lett. **75**, 1126 (1995); W. E. Pickett and D. J. Singh, Phys. Rev. B **53**, 1146 (1996).

[7] I. V. Solovyev, N. Hamada, and K. Terakura, Phys. Rev. B **53**, 7158 (1996).

[8] *A*- and *G*-type AFM structures correspond to the alternating ferromagnetic layers coupled antiferromagnetically along the (001) direction and AFM coupling for all the nearest Mn atoms, respectively.

[9] I. Dzyaloshinsky, J. Phys. Chem. Solids **4**, 241 (1958); T. Moriya, Phys. Rev. **120**, 91 (1960).

[10] R. Lorenz *et al.*, Phys. Rev. Lett. **74**, 3688 (1995); L. M. Sandratsii and J. Kübler, Phys. Rev. Lett. **75**, 946 (1995).

[11] A. I. Liechtenstein *et al.*, J. Magn. Magn. Mater. **67**, 65 (1987).

[12] I. V. Solovyev, P. H. Dederichs, and I. Mertig, Phys. Rev. B **52**, 13 419 (1995).

[13] Note that the formal electron configuration of Mn in $LaMnO_3$ is $t^3_{2g\uparrow} e^1_{g\uparrow}$.

[14] G. Matsumoto, J. Phys. Soc. Jpn. **29**, 606 (1970); J. B. A. A. Elemans *et al.*, J. Solid State Chem. **3**, 238 (1971).

[15] O. Gunnarsson, O. Jepsen, and O. K. Andersen, Phys. Rev. B **27**, 7144 (1983).

[16] The Brillouin zone integration (BZI) has been performed in the uniform grid generated by using 14 and 10 divisions along in-plane and perpendicular reciprocal-lattice vectors, respectively. Taking advantage of the work of P. E. Blöchl *et al.*, Phys. Rev. B **49**, 16 223 (1994), the BZI has been replaced by the weighted sums in the analogy of the special-point scheme. The energy integration has been performed in the complex plane by using 350 energy points on the rectangular contour. The choice of atomic spheres and LMTO basis is discussed in [7]. In order to improve the ASA description for exchange interactions, ΔV_{ex} has been estimated by using nonspherical distribution of the spin density inside the atomic sphere.

[17] V. Heine and J. H. Samson, J. Phys. F: Metal Phys. **13**, 2155 (1983).

[18] The transfer integrals are $t_{3x^2-r^2,3x^2-r^2} \simeq 1/4$, $t_{3x^2-r^2,y^2-z^2} \simeq \sqrt{3}/4$, and $t_{y^2-z^2,y^2-z^2} \simeq 3/4$ in terms of $(dd\sigma)$ two-center integral [J. C. Slater and G. F. Koster, Phys. Rev. **94**, 1498 (1954)].

[19] R. M. Bozorth, Phys. Rev. Lett. **1**, 362 (1958); D. Treves, Phys. Rev. **125**, 1843 (1962).